

Intrinsic breakdown strength: theoretical derivation and first-principles calculations

Shixu Liu,[†] Hongjun Xiang^{†‡}, Xin-Gao Gong^{†‡}, and Ji-Hui Yang^{†‡*}

[†]Key Laboratory of Computational Physical Sciences (Ministry of Education), Institute of Computational Physics, Fudan University, Shanghai 200433, China

[‡]Shanghai Qi Zhi Institute, Shanghai 200230, China

*corresponding author

Email: jhyang04@fudan.edu.cn

Abstract

Intrinsic breakdown strength (F_{bd}), as the theoretical upper limit of electric field strength that a material can sustain, plays important roles in determining dielectric and safety performance. The well accepted concept is that a larger band gap (E_g) often leads to a larger intrinsic breakdown strength. In this work, we analytically derive a simplified model of F_{bd} , showing a linear relationship between F_{bd} and the maximum electron density of states (DOS_{max}) within the energy range spanning from the conduction band minimum (CBM) to $\text{CBM} + E_g$. Using the Wannier interpolation technique to reduce the cost of calculating the F_{bd} for various three- and two-dimensional materials, we find that the calculated F_{bd} did not show any simple relationship with band gap, but it behaves linearly with the DOS_{max} , consistent with our theoretical derivation. Our work shows that the DOS_{max} is more fundamental than the band gap value in determining the F_{bd} , thus providing useful physical insights into the intrinsic dielectric breakdown strength and opening directions for improving high-power devices. The dimensional effects on F_{bd} has also been revealed that monolayers tend to have larger F_{bd} due to reduced screening effects.

KEYWORDS: intrinsic breakdown strength, first-principles, Wannier interpolation, electron-phonon coupling, maximum density of states, band gap, dimensional effects

Breakdown strength is a critical parameter in the design of electrical devices and systems, playing a pivotal role in determining both the dielectric and safety performance [1–4]. As the dimensions of electrical devices continue to shrink, and the demand for higher power increases, there is a growing focus on materials with exceptional breakdown strength, capable of operating under extremely high electric fields. Materials such as SiC, GaN, and diamond have garnered substantial attention due to their potential applications in high-power devices [5–8]. Moreover, in the realm of energy storage, supercapacitors necessitate materials with high breakdown strength to achieve elevated energy densities [1,9–16]. Despite the notable advancements in this field, a comprehensive understanding of the fundamental mechanisms governing breakdown strength remains a crucial pursuit.

Under an external electric field, electrons in a dielectric material gain energy from the field, and then lose energy due to scatterings by phonons or collisions with ions. Depending on how electrons dissipate energy, there are various breakdown mechanisms such as intrinsic, electromechanical, thermal, and electrochemical breakdown. For an intrinsic breakdown process, electrons lose energy only through electron-phonon scattering. Therefore, the intrinsic breakdown strength (denoted as F_{bd} hereafter) gives the upper boundary of the breakdown strength [17]. According to avalanche theory [18,19], at a low electric field, electrons have balanced rates of energy gain and loss. However, once the strength of the electric field exceeds the threshold, the average energy gain rate will become greater than the average energy loss rate, and the energy of electrons will continuously increase. As shown in Fig. 1, based on the von Hippel criterion [18], electrons that have an energy larger than the critical energy may collide with valence electrons, and excite them to the conductive bands, i.e., impact ionization. Consequently, the dielectric breakdown will happen. And for intrinsic breakdown, considering the energy conservation and momentum conservation, in direct band gap materials, the minimum energy required to excite a valence band electron to the conductive band is equal to the band gap (E_g) energy. For indirect band gap materials, this process may involve absorption or emission of phonons, but since phonon energy

are generally much smaller than the band gaps of dielectric materials, they can be neglected while dealing with energy conservation. Therefore, the critical energy is considered to be E_g here, which has been generally used in other works [20–22]. Note that, for some insulators that have band gaps larger than formation enthalpy (ΔH), like LiF, the critical energy should be ΔH to account for the stability issue [22]. Intuitively, the larger the band gap, the larger the F_{bd} [17,23,24]. Indeed, earlier models based on experimental data proposed a positive correlation between band gap and F_{bd} [25,26], and recent theoretical studies also showed that band gap and phonon cutoff frequency are significantly related to the intrinsic breakdown field, although these studies used relatively coarse \mathbf{q} -grids to sample the electron scattering [22,27]. The above insight has been a foundational consideration in the quest for increasing breakdown voltage and searching for dielectric materials with high breakdown strength [28–31]. Many works have tried to increase breakdown strength by increasing band gaps [12–14,32], however, the precise correlation between band gap values and intrinsic breakdown strength remains elusive. Consequently, a definitive consensus has yet to be reached on whether an increase in the band gap of a dielectric material invariably results in a commensurate enhancement of its intrinsic breakdown strength. Revealing this relationship is of great importance for gaining a comprehensive understanding of a material's performance under high electric field conditions, particularly for reliability in electronic devices and electrical equipment.

In this work, for the first time, we analytically derive that F_{bd} is linearly dependent on the maximum electron density of states (DOS_{max}) within the energy range spanning from the CBM to the CBM + E_g (for some materials is the CBM + ΔH due to the stability consideration) rather than the intuitive thought that F_{bd} is positively correlated to band gap value. Using first-principles methods in combination with the Wannier interpolation technique to efficiently sample the electron-phonon scatterings on very dense \mathbf{k} - and \mathbf{q} -grids, we accurately calculate F_{bd} for various systems ranging from three-dimensional crystals in different structures to two-dimensional (2D) monolayer

MoS₂ and phosphorene. For each system, we use different strains to tune its band gap as well as DOS_{max}. Our results show that, while the correlations between the F_{bd} and band gap values behave differently for different systems and lack a universal trend, the dependence of the F_{bd} on DOS_{max} consistently behaves linearly for every system studied, without exception, thus demonstrating our model.

The energy gain rate of the electron with energy E in a field F can be written as [22]

$$A(E, F) = \frac{e^2 \tau(E) F^2}{3m^*} \quad (1),$$

where e is the electronic charge and m^* is the effective electronic mass. The average electron relaxation time $\tau(E)$ is the reciprocal of the average electron scattering rate, given by

$$\frac{1}{\tau(E)} = \frac{1}{D(E)} \sum_{n\mathbf{k}} \frac{1}{\tau_{n\mathbf{k}}} \delta(\varepsilon_{n\mathbf{k}} - E) \quad (2),$$

where $D(E)$ is the density of states (DOS), and $\tau_{n\mathbf{k}}$ describes the process in which an electron in the initial state $|n\mathbf{k}\rangle$ is scattered by a phonon with frequency $\omega_{\mathbf{q}\nu}$, reaching the final state $|m\mathbf{k} + \mathbf{q}\rangle$. Using Fermi's golden rule, $\tau_{n\mathbf{k}}$ can be evaluated as

$$\begin{aligned} \frac{1}{\tau_{n\mathbf{k}}} = \frac{2\pi}{\hbar} \sum_{m\mathbf{q}\nu} & \left| g_{m\mathbf{k}+\mathbf{q},n\mathbf{k}}^{\mathbf{q}\nu} \right|^2 \left[n_{\mathbf{q}\nu} \delta(\varepsilon_{n\mathbf{k}} - \varepsilon_{m\mathbf{k}+\mathbf{q}} + \hbar\omega_{\mathbf{q}\nu}) \right. \\ & \left. + (n_{\mathbf{q}\nu} + 1) \delta(\varepsilon_{n\mathbf{k}} - \varepsilon_{m\mathbf{k}+\mathbf{q}} - \hbar\omega_{\mathbf{q}\nu}) \right] \quad (3), \end{aligned}$$

where $n_{\mathbf{q}\nu}$ is the Bose-Einstein distribution for phonons and the delta function ensures energy conservation. The electron-phonon coupling (EPC) matrix element $g_{m\mathbf{k}+\mathbf{q},n\mathbf{k}}^{\mathbf{q}\nu}$ is given by

$$g_{m\mathbf{k}+\mathbf{q},n\mathbf{k}}^{\mathbf{q}\nu} = \sqrt{\frac{\hbar}{2M\omega_{\mathbf{q}\nu}}} \left| \langle \psi_{m\mathbf{k}+\mathbf{q}} | \xi_{\mathbf{q}\nu} \cdot \nabla_{\mathbf{R}\mathbf{q}} | \psi_{n\mathbf{k}} \rangle \right|^2 \quad (4),$$

where M is the atomic mass, and ψ is the wave function of the electron. The phonon polarization vector is $\xi_{\mathbf{q}\nu}$, and $\nabla_{\mathbf{R}}V_{\mathbf{q}}$ is the gradient of the potential with respect to collective atomic displacements from their equilibrium positions \mathbf{R} .

The energy loss rate of the electron during a phonon absorption or emission process can be evaluated by [22]

$$B(E) = \frac{2\pi}{\hbar D(E)} \sum_{n\mathbf{k}} \sum_{m\mathbf{q}\nu} (\hbar\omega_{\mathbf{q}\nu}) \left| g_{m\mathbf{k}+\mathbf{q},n\mathbf{k}}^{\mathbf{q}\nu} \right|^2 \left[(n_{\mathbf{q}\nu} + 1) \delta(\varepsilon_{n\mathbf{k}} - \varepsilon_{m\mathbf{k}+\mathbf{q}} - \hbar\omega_{\mathbf{q}\nu}) - n_{\mathbf{q}\nu} \delta(\varepsilon_{n\mathbf{k}} - \varepsilon_{m\mathbf{k}+\mathbf{q}} + \hbar\omega_{\mathbf{q}\nu}) \right] \delta(\varepsilon_{n\mathbf{k}} - E) \quad (5).$$

Then, using the von Hippel breakdown criterion [18], i.e.,

$$A(E, F) > B(E), \quad E \in [\text{CBM}, \text{CBM} + E_g] \quad (6),$$

one can obtain

$$F_{\text{bd}} = \text{Max} \left[\frac{\sqrt{3m^*}}{e} \sqrt{\frac{1}{\tau(E)} B(E)} \right], \quad E \in [\text{CBM}, \text{CBM} + E_g] \quad (7).$$

As seen from Eqs. (1)-(7), the band gap value is not directly utilized in the calculation of F_{bd} . To determine the intrinsic breakdown field, we focus on the summation term of the electron energy by using an averaged phonon frequency and EPC strength to replace the momentum-dependent ω and g terms. Note that the utilization of this approximation concept is prevalent in the field of superconductivity [33]. In this case, we rewrite Eqs. (2) and (5) (see the Supplemental Materials for the derivation [34]) as

$$\frac{1}{\tau(E)} = \frac{1}{\tau_{\mathbf{k}}} = \frac{2\pi}{\hbar} g_{\text{eff}}^2 (2n_0 + 1) D(E) \quad (8), \quad \text{and}$$

$$B(E) = \frac{2\pi}{\hbar} (\hbar\omega_{\text{mean}}) g_{\text{eff}}^2 D(E) \quad (9),$$

where $\hbar\omega_{\text{mean}}$ represents the average energy for phonons that participate in the scattering process, n_0 is the average occupation number of phonons, and g_{eff} is the

average EPC strength. As we can see, $\frac{1}{\tau(E)}$ and $B(E)$ are roughly proportional to $D(E)$.

Accordingly, F_{bd} can be expressed as

$$F_{\text{bd}} = \frac{\sqrt{3m^*} 2\pi}{e \hbar} g_{\text{eff}}^2 \sqrt{(2n_0 + 1)\hbar\omega_{\text{mean}}} \text{DOS}_{\text{max}} \quad (10).$$

Thus, we have a linear relationship between F_{bd} and DOS_{max} if the remaining terms do not change much in a given material.

To demonstrate the above model, we calculate the intrinsic breakdown field strengths for various materials with diverse atomic structures, band structures and symmetries, including diamond and silicon in the diamond structure, ZnO (ZB-ZnO), AlAs, and SiC (ZB-SiC) in the zinc blende structure, GaN (W-GaN) in the wurtzite structure, LiF and NaCl in the NaCl-type structure, CsCl in the CsCl-type structure, as well as MoS₂ and phosphorene in the monolayer structure (m-MoS₂ and BP). The calculation details can be found in the Supplementary Materials [34]. To ensure calculation accuracy, relatively dense \mathbf{k} - and \mathbf{q} -grids are often needed for sampling in the Brillouin zone, which is very expensive. To reduce the computational cost, we first obtain necessary quantities on relatively sparse grids and then we adopt the Wannier interpolation technique to obtain band structures, phonon dispersions and EPC matrices on the fine grids. Convergence tests are conducted on these materials (see Supplementary Materials [34] for more details). In the following studies, we set the sizes of both \mathbf{k} - and \mathbf{q} -grids as $100 \times 100 \times 100$ for the bulk systems (for W-GaN, we use $100 \times 100 \times 60$ mesh), $300 \times 300 \times 1$ for m-MoS₂ and $320 \times 240 \times 1$ for BP. The smearing parameter is set at 0.01 eV. In general, the computational cost tends to increase rapidly with the density of the grid. Therefore, the utilization of the Wannier interpolation technique is indispensable and highly efficient for achieving a balance between accuracy and cost. Note that the electric field is assumed to be applied in the in-plane direction for 2D materials and BP exhibits strong anisotropic band structure near the CBM with the effective masses being 1.24 and 0.07 m_e along the zigzag and armchair directions, respectively. Therefore, we use the geometric mean value $m^* =$

$\sqrt{m_X^* m_Y^*}$ to estimate the effective mass in Eq. (7). The hydrostatic strain in bulk materials is applied by directly changing the lattice constant, which is defined as $(a - a_0)/a_0$, where a and a_0 are the lattice constants with and without strain, respectively. While in 2D materials, biaxial strain is applied. To deal with the underestimation of band gaps under the Perdew-Burke-Ernzerhof exchange-correlation functional [36], we correct them using experimental values, i.e., $E_g^* = E_g - E_g^{\text{ref}} + E_g^{\text{exp}}$, where E_g^{exp} is the experimental band gap, E_g and E_g^{ref} are the calculated band gaps with and without strain, respectively. Using our recently developed machine learning method [40], we also use the HSE functional [41] to get more accurate band structures and EPC matrices to calculate the F_{bd} .

Our calculated results are shown in Table I and Table SI. And the calculated F_{bd} are in good agreement with previous theoretical results [22,27] and available experimental measurements. An interesting finding is that ZB-ZnO has an even smaller F_{bd} than Si despite its much larger band gap, which completely violates the prevailing view. Note that, F_{bd} is not only correlated to E_g but also depends on the electron effective mass and EPC. To focus on revealing the correlation between F_{bd} and E_g , we use strains to manipulate the bandgaps and study the dependence of F_{bd} on bandgaps for each system. For bulk materials, the strains cover from -2% to +2%. For m-MoS₂, the strains cover from 0 to +2%, and for BP, the strains are in the range between -1% to 2%. Our calculation results are shown in Fig. 2. The results of more materials can be found in the Supplemental Materials [32]. For Si and BP, we find that the band gaps increase with increasing strain, which is consistent with previous results [51–55]. In contrast, for diamond [56], ZB-ZnO and m-MoS₂ [57], the bandgaps decrease with increasing strain. As for the relationship between bandgap and F_{bd} , we can see in Fig. 2(a)-(e) that only the results for Si and ZB-ZnO are consistent with the common view, whereas for other materials, the common view does not hold, especially for diamond and m-MoS₂.

In general, our results show that there is no clear dependence of F_{bd} on band gap value, suggesting the absence of a universal trend.

Next, we examine the correlation between F_{bd} and DOS_{max} . To eliminate the strain effects on effective masses and phonon frequencies, we normalize DOS_{max} by multiplying by the M factor, i.e., $M = \sqrt{m^* \omega_{\text{mean}}}$, for each material under different strains (see also Eq. 10) and we use ω_{cutoff} to approximate ω_{mean} here. The relationships between $M\text{DOS}_{\text{max}}$ and F_{bd} are shown in Fig. 2(f)-(j). It is clearly seen that F_{bd} is linearly dependent on the normalized DOS_{max} for every system without exception, thus demonstrating our model. The slight deviation from linearity is mainly due to the variation of the g_{eff}^2 term under different strains.

To ascertain why the common view is flawed, we analyze the energy gain rates and energy loss rates for unstrained materials. As shown in Fig. 3, under a given electric field, electrons with low energies have higher energy gain rates compared to their energy loss rates. Consequently, the electron energy will increase until it reaches a pinning energy (PE) above which the energy loss rate exceeds the energy gain rate. For example, the PE for Si under an electric field of 63.9 MV/m is 0.95 eV, as shown in Fig. 3(a). Electrons with lower energies will undergo a net energy gain, while those with higher energies will experience a net energy loss. Thus, the average energy of electrons will be equal to the PE. With an increasing electric field, the PE also increases for Si, since the energy loss rate increases and the energy gain rate decreases monotonically with electron energy increasing from the CBM to the $\text{CBM} + E_g$, as seen in Fig. 3(a). Consequently, the PE also increases monotonically with the increasing electric field. When the PE reaches the maximum, that is, $\text{CBM} + E_g$, which is 1.17 eV for Si, conducting electrons will have sufficient energies to excite valance electrons into conduction bands, leading to breakdown. The increase in E_g will lead to a corresponding increase in the PE maximum, thereby allowing for a larger electric field, that is, enhancement of F_{bd} . Therefore, the thought that a larger band gap leads to a

larger F_{bd} holds for Si. A similar situation exists for ZB-ZnO [see Fig. S2(a)], in which the PE maximum is also located at $\text{CBM} + E_g$ exactly under the breakdown field.

For diamond, however, we find that neither the energy loss rate nor the energy gain rate changes monotonically with electron energy increasing from the CBM to the $\text{CBM} + E_g$. As seen in Fig. 3(b), the energy loss rate has a peak and the energy gain rate has a dip around 4.3 eV. When the PE is smaller than 4.3 eV, the electron energies will be pinned by the PE and the breakdown will not happen. With further increase of the electric field, the PE of electrons increases. When the electric field reaches 2972.6 MV/m, the PE will reach 4.3 eV. Under this field, the energies of electrons will exceed 4.3 eV and keep increasing because the energy gain rate is always larger than the energy loss rate when the electron energy is larger than 4.3 eV. Ultimately, the electrons will have energies larger than the $\text{CBM} + E_g$, leading to breakdown. In this case, the F_{bd} is not directly related to the E_g but is determined by the PE maximum. As a larger E_g does not necessarily lead to a larger PE maximum, the prevailing thought that a larger band gap leads to a larger F_{bd} fails for diamond. Similar situations happen for m-MoS₂ and BP in which the PE maxima appear before $\text{CBM} + E_g$ [see Figs. S2(b) and S2(c)].

Note that, according to our model, the energy loss rate and gain rate reach the maximum and minimum, respectively, when the DOS reaches DOS_{max} according to Eqs. (8) and (9). The consequence is that, with the increase of electric field strength before breakdown, the intersection will finally happen at the position of the DOS_{max} , which determines the PE maximum and thus the F_{bd} . For systems such as Si, the DOS increases monotonically with electron energy and reaches the maximum at the $\text{CBM} + E_g$. Therefore, if strain induces an increase in the band gap, it also results in a corresponding enhancement of DOS_{max} , leading to a larger F_{bd} . In this case, the prevailing view is valid. For systems such as diamond, the DOS_{max} is reached before the electron energy reaches the $\text{CBM} + E_g$, as seen in Fig. S3(d). Although the tensile

strain reduces the band gap, the DOS_{max} still increases. The consequence is that the F_{bd} gets larger counterintuitively. In this case, the prevailing view fails. Our results show that, it is the DOS_{max} rather than the commonly believed band gap that plays the dominant role in determining F_{bd} .

Through our model, we can explain why ZB-ZnO has a smaller F_{bd} than Si despite its larger experimental band gap of 3.27 eV [58] compared to 1.17 eV for Si. The band structure of ZB-ZnO shows that there is simply one band, mainly consisting of an s-orbital of Zn between the CBM and the $\text{CBM} + E_{\text{g}}$, as shown in Fig. S4. Hence, the DOS_{max} of ZB-ZnO is much smaller than that of Si, i.e., 0.22 v.s. 0.94, leading to the relatively low F_{bd} in ZB-ZnO.

In addition, we can reveal the dimensional effects on the F_{bd} , since low-dimensional materials tend to suffer high electric field under operations. Generally speaking, dimensional effect is mainly manifested in the quantum confinement effect and reduction of screening effect. On the one hand, the quantum confinement effect will generally lead to the increase of the band gap values in monolayers and thus will affect the DOS_{max} between CBM and $\text{CBM} + E_{\text{g}}$. However, whether DOS_{max} will be larger or not in monolayers has no decisive conclusions. On the other hand, due to the reduced screening effect, EPC are often stronger in monolayers, which is good for obtaining larger F_{bd} . Taking MoS_2 as an example, we compare the breakdown field strength for monolayer and bulk phase in the Supplementary Materials [34]. We find that the calculated F_{bd} of monolayer MoS_2 is larger than that of bulk phase, in agreement with experimental results [50]. However, the larger F_{bd} in monolayer MoS_2 is actually mainly due to the stronger EPC rather than the increased band gap.

Finally, we want to mention that, to get more accurate F_{bd} , it is necessary to use accurate band structures and EPC matrices using more advanced functionals. We have discussed the calculated F_{bd} using different functionals in the Supplementary Materials [34], and the results show that HSE functional can provide more reasonable results compared to

experiments for some systems. Nevertheless, our model and our conclusion, which are not limited to the choice of special functionals, will not be quantitatively affected.

In conclusion, we have developed an analytical model that shows a linear relationship between F_{bd} and DOS_{max} using appropriate approximations. To accurately determine the value of F_{bd} within a reasonable time, we employed the Wannier interpolation technique in our calculations and showed the necessity of using dense \mathbf{k} - and \mathbf{q} -meshes to achieve convergence. By investigating the behaviors of F_{bd} under different strains in different materials, we found that F_{bd} has no clear dependence on band gap value and validated the effectiveness of our model even in cases where the prevailing view does not hold. Our work shows that the DOS_{max} is more fundamental than the band gap value in determining the F_{bd} and suggests that F_{bd} might be enhanced by engineering the DOS using strategies like strain and doping, opening directions for improving high-power devices.

ACKNOWLEDGMENTS

This work was partially supported by the Guangdong Major Project of the Basic and Applied Basic Research (Future functional materials under extreme conditions 2021B0301030005), the China National Key R&D Program (2022YFA1404603), and the National Natural Science Foundation of China (Grants No. 12188101 and No. 11991061).

Table I. Calculated properties of Si, diamond, ZB-ZnO, m-MoS₂ and BP. The experimental values are obtained from ref [17,49,50,59–61].

System	a_0 (Å)	b_0 (Å)	E_g (eV)	E_g^{exp} (eV)	m^* (m_e)	F_{bd} (MV/m)	$F_{\text{bd}}^{\text{exp}}$ (MV/m)
Si	5.469		0.608	1.17 ^a	0.959	79.9	50 ^e
Diamond	3.572		4.173	5.48 ^a	1.642	2972.6	2150 ^e
ZB-ZnO	4.620		0.699	3.27 ^b	0.128	71.0	----
m-MoS ₂	3.185		1.658	1.90 ^c	0.447	225.8	433 ^f
BP	3.303	4.625	0.894	2.00 ^d	0.294	212.8	----

^aReference [59]

^bReference [60]

^cReference [49]

^dReference [61]

^eReference [17]

^fReference [50]

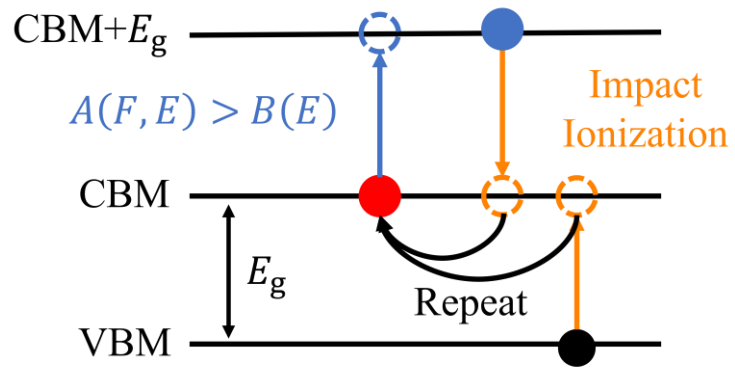


FIG. 1. Schematic diagram for the process of electron avalanche breakdown.

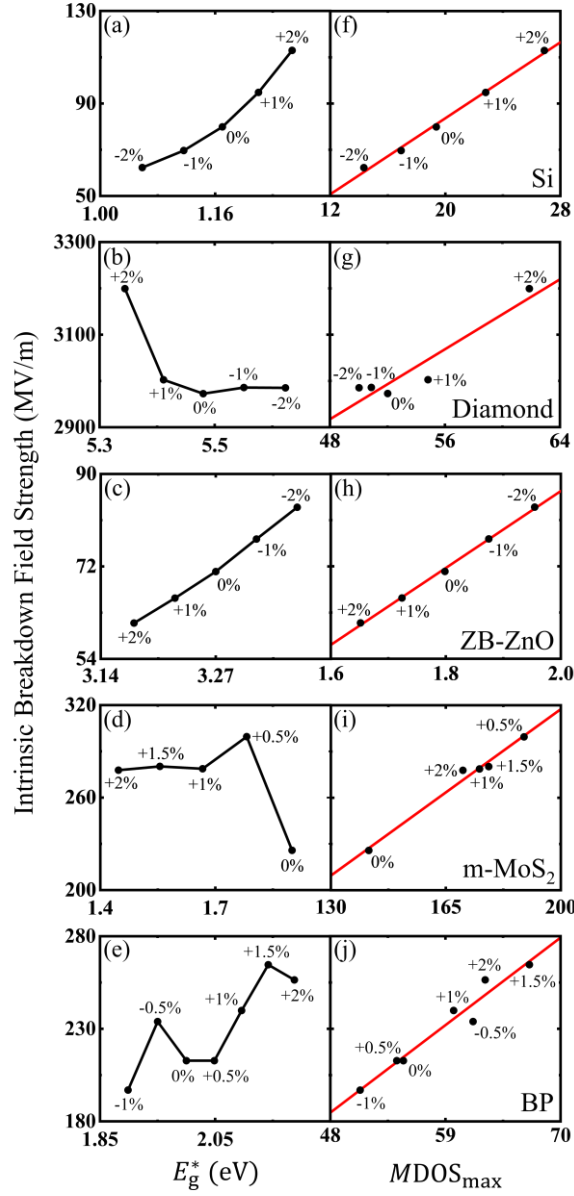


FIG. 2. Comparison of the relation between F_{bd} and band gap with that between F_{bd} and $MDOS_{max}$. Here, the band gap and DOS_{max} are tuned using strains, which are labeled for each data. The calculated F_{bd} as a function of E_g^* for strained (a) Si, (b) diamond, (c) ZB-ZnO, (d) m-MoS₂ and (e) BP, respectively. The relationships between F_{bd} and $MDOS_{max}$ for strained (f) Si, (g) diamond, (h) ZB-ZnO, (i) m-MoS₂ and (j) BP, respectively. The red lines are the results of linear fitting for eye guide. Note that, the calculated F_{bd} did not follow a simple relationship with the band gap, while the linear dependence of F_{bd} on the $MDOS_{max}$ holds for every system.

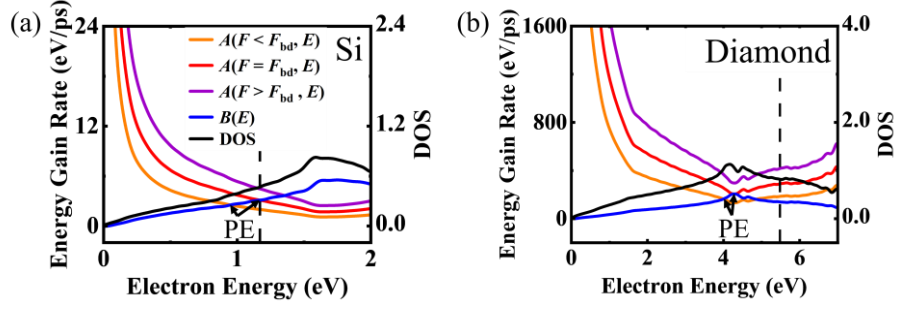


FIG. 3. The calculated breakdown properties for Si and diamond. The calculated energy gain rates, energy loss rates and DOS for (a) Si and (b) diamond. The red line is the energy gain rate under the external field of F_{bd} , while the yellow and purple line correspond to the energy gain rates when the external field is 20% smaller and larger than F_{bd} , respectively. The electron energy scale is referenced to the CBM and the vertical dotted lines represent the band gaps. Notably, the curve shapes of the energy gain rate and energy loss rate indicate that they are closely related to DOS, and the intersection of them does not necessarily locate at $CBM + E_g$ under the breakdown field.

Reference:

- [1] J. Kim, S. Saremi, M. Acharya, G. Velarde, E. Parsonnet, P. Donahue, A. Qualls, D. Garcia, and L. W. Martin, Ultrahigh capacitive energy density in ion-bombarded relaxor ferroelectric films, *Science* **369**, 81 (2020).
- [2] A. Ranjan, N. Raghavan, M. Holwill, K. Watanabe, T. Taniguchi, K. S. Novoselov, K. L. Pey, and S. J. O'Shea, Dielectric breakdown in single-crystal hexagonal boron nitride, *ACS Appl. Electron. Mater.* **3**, 3547 (2021).
- [3] F. Palumbo, C. Wen, S. Lombardo, S. Pazos, F. Aguirre, M. Eizenberg, F. Hui, and M. Lanza, A review on dielectric breakdown in thin dielectrics: Silicon dioxide, high-k, and layered dielectrics, *Adv. Funct. Mater.* **30**, 1900657 (2020).
- [4] J. Y. Tsao et al., Ultrawide-Bandgap Semiconductors: Research Opportunities and Challenges, *Adv. Electron. Mater.* **4**, 1600501 (2018).
- [5] S. Nakamura, H. Kumagai, T. Kimoto, and H. Matsunami, Anisotropy in breakdown field of 4H-SiC, *Appl. Phys. Lett.* **80**, 3355 (2002).
- [6] T. P. Chow, High-voltage SiC and GaN power devices, *Microelectronic Engineering* **83**, 112 (2006).
- [7] R. Singh, Reliability and performance limitations in SiC power devices, *Microelectronics Reliability* **46**, 713 (2006).
- [8] H. Umezawa, M. Nagase, Y. Kato, and S. Shikata, High temperature application of diamond power device, *Diamond and Related Materials* **24**, 201 (2012).
- [9] Z. Jiang, B. Xu, H. Xiang, and L. Bellaiche, Ultrahigh energy storage density in epitaxial AlN/ScN superlattices, *Phys. Rev. Mater.* **5**, L072401 (2021).
- [10] B. Xu, J. Íñiguez, and L. Bellaiche, Designing lead-free antiferroelectrics for energy storage, *Nat. Commun.* **8**, 15682 (2017).
- [11] Z. Yao, Z. Song, H. Hao, Z. Yu, M. Cao, S. Zhang, M. T. Lanagan, and H. Liu, Homogeneous/Inhomogeneous-structured dielectrics and their energy-storage performances, *Adv. Mater.* **29**, 1601727 (2017).
- [12] M. H. Park, H. J. Kim, Y. J. Kim, T. Moon, K. D. Kim, and C. S. Hwang, Thin Hf_xZr_{1-x}O₂ films: A new lead-free system for electrostatic supercapacitors with large energy storage density and robust thermal stability, *Adv. Energy Mater.* **4**, 1400610 (2014).
- [13] R. Ma, A. F. Baldwin, C. Wang, I. Offenbach, M. Cakmak, R. Ramprasad, and G. A. Sotzing, Rationally designed polyimides for high-energy density capacitor applications, *ACS Appl. Mater. Interfaces* **6**, 10445 (2014).
- [14] W.-C. Zhang, H. Wu, W.-F. Sun, and Z.-P. Zhang, First-principles study of n*AlN/n*ScN superlattices with high dielectric capacity for energy storage, *Nanomaterials* **12**, 1966 (2022).
- [15] Q. Li, F.-Z. Yao, Y. Liu, G. Zhang, H. Wang, and Q. Wang, High-temperature dielectric materials for electrical energy storage, *Annu. Rev. Mater. Res.* **48**, 219 (2018).
- [16] B. Peng et al., Giant electric energy density in epitaxial lead-free thin films with coexistence of ferroelectrics and antiferroelectrics, *Adv. Electron. Mater.* **1**, 1500052 (2015).
- [17] Y. Sun, C. Bealing, S. Boggs, and R. Ramprasad, 50+ years of intrinsic breakdown, *IEEE Electr. Insul. Mag.* **29**, 8 (2013).
- [18] A. Von Hippel, Electric breakdown of solid and liquid insulators, *J. Appl. Phys.* **8**, 815 (1937).
- [19] M. Sparks, D. L. Mills, R. Warren, T. Holstein, A. A. Maradudin, L. J. Sham, E. Loh, and D. F. King, Theory of electron-avalanche breakdown in solids, *Phys. Rev. B* **24**, 3519 (1981).

- [20] H. Fröhlich, Theory of electrical breakdown in ionic crystals, Proc. R. Soc. Lond. A **160**, 230 (1937).
- [21] H. Fröhlich, Dielectric breakdown in solids, Rep. Prog. Phys. **6**, 411 (1939).
- [22] Y. Sun, S. A. Boggs, and R. Ramprasad, The intrinsic electrical breakdown strength of insulators from first principles, Appl. Phys. Lett. **101**, 132906 (2012).
- [23] R. Ma, V. Sharma, A. F. Baldwin, M. Tefferi, I. Offenbach, M. Cakmak, R. Weiss, Y. Cao, R. Ramprasad, and G. A. Sotzing, Rational design and synthesis of polythioureas as capacitor dielectrics, J. Mater. Chem. A **3**, 14845 (2015).
- [24] Z. Li, C. Wu, L. Chen, Y. Wang, Z. Mutulu, H. Uehara, J. Zhou, M. Cakmak, R. Ramprasad, and Y. Cao, Probing electronic band structures of dielectric polymers via pre-breakdown conduction, Adv. Mater. 2310497 (2024).
- [25] J. L. Hudgins, G. S. Simin, E. Santi, and M. A. Khan, An assessment of wide bandgap semiconductors for power devices, IEEE Trans. Power Electron. **18**, 907 (2003).
- [26] Li-Mo Wang, *Relationship between Intrinsic Breakdown Field and Bandgap of Materials*, in *2006 25th International Conference on Microelectronics* (IEEE, Belgrade, Serbia and Montenegro, 2006), pp. 576–579.
- [27] C. Kim, G. Pilia, and R. Ramprasad, From organized high-throughput data to phenomenological theory using machine learning: The example of dielectric breakdown, Chem. Mater. **28**, 1304 (2016).
- [28] C. Kim, G. Pilia, and R. Ramprasad, Machine learning assisted predictions of intrinsic dielectric breakdown strength of ABX₃ perovskites, J. Phys. Chem. C **120**, 14575 (2016).
- [29] V. Sharma et al., Rational design of all organic polymer dielectrics, Nat. Commun. **5**, 4845 (2014).
- [30] A. Alamri, C. Wu, S. Nasreen, H. Tran, O. Yassin, R. Gentile, D. Kamal, R. Ramprasad, Y. Cao, and G. Sotzing, High dielectric constant and high breakdown strength polyimide *via* tin complexation of the polyamide acid precursor, RSC Adv. **12**, 9095 (2022).
- [31] J. Kern, L. Chen, C. Kim, and R. Ramprasad, Design of polymers for energy storage capacitors using machine learning and evolutionary algorithms, J. Mater. Sci. **56**, 19623 (2021).
- [32] C.-W. Lee, N. U. Din, K. Yazawa, G. L. Brennecke, A. Zakutayev, and P. Gorai, Emerging materials and design principles for wurtzite-type ferroelectrics, Matter **7**, 1644 (2024).
- [33] P. B. Allen and R. C. Dynes, Transition temperature of strong-coupled superconductors reanalyzed, Phys. Rev. B **12**, 905 (1975).
- [34] See Supplemental Material for the detail derivation, results for other materials, calculation method, convergence test results, discussions of dimensional effects and different functionals, and also the dependence on temperature, which includes Refs. [17,20,22,35–50].
- [35] D. R. Hamann, Optimized norm-conserving Vanderbilt pseudopotentials, Phys. Rev. B **88**, 085117 (2013).
- [36] J. P. Perdew, K. Burke, and M. Ernzerhof, Generalized gradient approximation made simple, Phys. Rev. Lett. **77**, 3865 (1996).
- [37] P. Giannozzi et al., QUANTUM ESPRESSO: a modular and open-source software project for quantum simulations of materials, J. Phys.: Condens. Matter **21**, 395502 (2009).
- [38] J.-J. Zhou, J. Park, I.-T. Lu, I. Maliyov, X. Tong, and M. Bernardi, Perturbo: A software package for ab initio electron–phonon interactions, charge transport and ultrafast dynamics, Comput. Phys. Commun. **264**, 107970 (2021).

- [39] W. L. Smith, J. H. Bechtel, and N. Bloembergen, Dielectric-breakdown threshold and nonlinear-refractive-index measurements with picosecond laser pulses, *Phys. Rev. B* **12**, 706 (1975).
- [40] Y. Zhong, S. Liu, B. Zhang, Z. Tao, Y. Sun, W. Chu, X.-G. Gong, J.-H. Yang, and H. Xiang, Accelerating the calculation of electron–phonon coupling strength with machine learning, *Nat. Comput. Sci.* **4**, 615 (2024).
- [41] J. Heyd, G. E. Scuseria, and M. Ernzerhof, Hybrid functionals based on a screened Coulomb potential, *J. Chem. Phys.* **118**, 8207 (2003).
- [42] A. E. W. Austen and S. Whitehead, The electric strength of some solid dielectrics, *Proc. R. Soc. Lond. A* **176**, 33 (1940).
- [43] K. Karch, F. Bechstedt, P. Pavone, and D. Strauch, Pressure-dependent properties of SiC polytypes, *Phys. Rev. B* **53**, 13400 (1996).
- [44] H. Jin, G. L. Zhao, and D. Bagayoko, Density functional band gaps of AlAs, *Phys. Rev. B* **73**, 245214 (2006).
- [45] C. Caetano, L. K. Teles, M. Marques, A. Dal Pino, and L. G. Ferreira, Phase stability, chemical bonds, and gap bowing of $\text{In}_x\text{Ga}_{1-x}\text{N}$ alloys: Comparison between cubic and wurtzite structures, *Phys. Rev. B* **74**, 045215 (2006).
- [46] T. Ono and K. Hirose, First-principles study of dielectric properties of bulk NaCl and ultrathin NaCl films under a finite external electric field, *Phys. Rev. B* **72**, 085105 (2005).
- [47] A. Ejiri and K. Arakaki, Vacuum UV photoelectric yield and photoluminescence in CsCl and CsBr, *Solid State Commun.* **110**, 575 (1999).
- [48] M. Abe, H. Nagasawa, P. Ericsson, H. Strömberg, M. Bakowski, and A. Schöner, High current capability of 3C-SiC vertical DMOSFETs, *Microelectron. Eng.* **83**, 24 (2006).
- [49] K. F. Mak, C. Lee, J. Hone, J. Shan, and T. F. Heinz, Atomically thin MoS_2 : A new direct-gap semiconductor, *Phys. Rev. Lett.* **105**, 136805 (2010).
- [50] J. Pak et al., Two-dimensional thickness-dependent avalanche breakdown phenomena in MoS_2 field-effect transistors under high electric fields, *ACS Nano* **12**, 7109 (2018).
- [51] B. Welber, C. K. Kim, M. Cardona, and S. Rodriguez, Dependence of the indirect energy gap of silicon on hydrostatic pressure, *Solid State Commun.* **17**, 1021 (1975).
- [52] M. Alouani and J. M. Wills, Calculated optical properties of Si, Ge, and GaAs under hydrostatic pressure, *Phys. Rev. B* **54**, 2480 (1996).
- [53] Z. Xie, L. Hui, J. Wang, G. Zhu, Z. Chen, and C. Li, Electronic and optical properties of monolayer black phosphorus induced by bi-axial strain, *Comput. Mater. Sci.* **144**, 304 (2018).
- [54] D. Çakır, H. Sahin, and F. M. Peeters, Tuning of the electronic and optical properties of single-layer black phosphorus by strain, *Phys. Rev. B* **90**, 205421 (2014).
- [55] C. Kim and R. Ramprasad, Dielectric breakdown field of strained silicon under hydrostatic pressure, *Appl. Phys. Lett.* **111**, 112904 (2017).
- [56] M. P. Surh, S. G. Louie, and M. L. Cohen, Band gaps of diamond under anisotropic stress, *Phys. Rev. B* **45**, 8239 (1992).
- [57] L. Dong, R. R. Namburu, T. P. O'Regan, M. Dubey, and A. M. Dongare, Theoretical study on strain-induced variations in electronic properties of monolayer MoS_2 , *J. Mater. Sci.* **49**, 6762 (2014).
- [58] A. A. Ashrafi, A. Ueta, H. Kumano, and I. Suemune, Role of ZnS buffer layers in growth of zincblende ZnO on GaAs substrates by metalorganic molecular-beam epitaxy, *J. Cryst. Growth* **221**, 435 (2000).
- [59] F. Tran and P. Blaha, Accurate band gaps of semiconductors and insulators with a semilocal

exchange-correlation potential, Phys. Rev. Lett. **102**, 226401 (2009).

[60] H. I. Berrezoug, A. E. Merad, A. Zerga, and Z. S. Hassoun, Simulation and modeling of structural stability, electronic structure and optical properties of ZnO, Energy Procedia **74**, 1517 (2015).

[61] X.-B. Li, P. Guo, T.-F. Cao, H. Liu, W.-M. Lau, and L.-M. Liu, Structures, stabilities and electronic properties of defects in monolayer black phosphorus, Sci. Rep. **5**, 10848 (2015).

[62] B. J. Abdullah, Size effect of band gap in semiconductor nanocrystals and nanostructures from density functional theory within HSE06, Mater. Sci. Semicond. Process. **137**, 106214 (2022).

[63] Y.-S. Kim, M. Marsman, G. Kresse, F. Tran, and P. Blaha, Towards efficient band structure and effective mass calculations for III-V direct band-gap semiconductors, Phys. Rev. B **82**, 205212 (2010).